

# How slowly do run-and-tumble bacteria approach the diffusive regime?

Andrea Villa-Torrealba,\* Cristóbal Chávez Raby, Pablo de Castro,† and Rodrigo Soto‡

*Departamento de Física, Facultad de Ciencias Físicas y Matemáticas,  
Universidad de Chile, Avenida Blanco Encalada 2008, Santiago, Chile*

(Dated: February 10, 2020)

The run-and-tumble (RT) dynamics followed by bacterial swimmers gives rise first to a ballistic motion due to their persistence, and later, through consecutive tumbles, to a diffusive process. Here we investigate how long it takes for a dilute swimmer suspension to reach the diffusive regime as well as what is the amplitude of the deviations from the diffusive dynamics, which we characterize by the excess kurtosis of the displacement distribution. Four swimming strategies are considered: (i) the conventional RT model with complete reorientation after tumbling, (ii) the case of partial reorientation, characterized by a distribution of tumbling angles, (iii) a run-and-reverse model with rotational diffusion, and (iv) a RT particle where the tumbling rate depends on the stochastic concentration of an internal protein. By analyzing the associated kinetic equations for the probability density function and simulating the models, we find that for models (ii), (iii), and (iv) the relaxation to diffusion can take much longer than the mean time between tumble events, evidencing the existence of large tails in the particle displacements. Moreover, the kurtosis can assume large positive values. In model (ii) it is possible for some distributions of tumbling angles that the mean-squared displacement increases linearly with time but, still, the dynamics remains non-Gaussian for long times. For all models, the long-time diffusion coefficients are also obtained. The theoretical approach, which relies on eigenvalue expansions of the van Hove function, is in excellent agreement with the simulations.

## I. INTRODUCTION

There are billions of different species of bacteria on Earth [1]. Because of adaptation, their life and swimming styles vary across a multitude of distinct environments and conditions [2, 3]. The vast majority have never been researched, and are thus dubbed *Microbial Dark Matter* [4]. On the other hand, the *E. coli* bacteria continue to be extensively studied. Their motion is usually modeled as a run-and-tumble (RT) dynamics. In fact, their flagella can rotate and propel the cell body in a “run” mode which can suddenly terminate whenever some of them reverse direction [5]. This leads to a quick reorientation mode called “tumble”—which is then followed by another run—with an average tumbling angle of approximately  $70^\circ$  [6]. In the case of marine bacteria, up to 70% of them are thought to have a distribution of tumbling angles peaked around  $180^\circ$  instead [7]. Examples include *S. putrefaciens* and *P. haloplanktis* [8], and thus in this case we speak of a run-and-reverse motion.

In his seminal work [9, 10], Berg showed that bacteria and other microswimmers performing run-and-tumble motion develop, in the long term, a diffusive motion. If  $V$  is the characteristic run velocity and  $\nu_0$  the tumble rate (or rotational diffusion coefficient for the case of smooth runners), the diffusion coefficient scales as  $D \sim V^2/\nu_0$ , with a prefactor that depends on the tumble properties. For example, in the case of three-dimensional Markovian swimmers, i.e., each tumble is uncorrelated from previ-

ous ones and tumble events are distributed as a Poisson process,  $D = V^2/[3\nu_0(1 - \langle \cos \theta_s \rangle)]$ , where  $\theta_s$  is the tumbling (or “scattering”) angle between the pre- and post-tumble directors [9, 10]. The diffusive regime is extensively used in chemical and environmental engineering to describe the spatiotemporal spreading of bacteria using reaction–diffusion equations [11–13]. At short times, on the other hand, the swimmers’ persistent motion give rise to a ballistic motion. Naïvely, the crossover time between the ballistic and diffusive regimes is expected to scale as  $\nu_0^{-1}$ . In this article we thoroughly show that, in some cases, the prefactor can be quite large and thus the non-diffusive regime can persist for long times.

Here, we consider several run-and-tumble models which are distinct in swimming strategy and compare how slowly these microswimmers approach the diffusive regime. Our motivation is to quantitatively study the dispersal process of bacteria. The swimming strategies considered here are different not only in terms of the distribution of tumbling angles but in whether or not the tumbling rate remains constant over time. In particular we consider the Tu–Grinstein model [14] where the concentration of a phosphorylated internal protein named CheY-P changes stochastically with time [15], affecting the tumbling rate exponentially. Previous studies have discussed departures from diffusion by using the mean-squared displacement (MSD) for run-and-tumble swimmers with anomalous diffusion [16] and for deformable active Brownian particles (ABPs) [17]. Other types of ABPs have also been analyzed through the excess kurtosis of the displacement distribution [18, 19]. Ref. [20] has recently studied the non-Gaussian behavior of interacting run-and-tumble particles in the context of active polymer chains and lattice models, where the authors have employed analytical methods which are based on solving

\* aavillat@gmail.com

† pdecastro@ing.uchile.cl

‡ rsoto@dfi.uchile.cl

the associated Langevin equation and considered simpler tumbling processes. Our analysis is done by performing simulations and derivations of both the MSD and the excess kurtosis for the different RT models, aiming to determine how long the system takes to reach the diffusive regime. The analytical part is carried out from associated kinetic equations, with Fokker-Planck terms to describe rotational diffusion and the evolution of the internal protein [21] coupled with a Lorentz term to account for the tumbling [22–24]. The simulations are essentially numerical solutions of the stochastic differential equations of motion, i.e., Langevin dynamics. In all cases, we will consider two spatial dimensions.

The paper is organized as follows. Section II brings our review and further development of general theoretical aspects that will be used throughout the paper. In Section III we consider three distinct swimming strategies with constant tumbling rate. Section IV brings a thorough analysis of the case with stochastic tumbling rate. Finally, our conclusions and a discussion are presented in Section V.

## II. GENERAL THEORETICAL ASPECTS

We start by presenting commonly used model-independent expressions which will be essential in the following sections. From these results we will then derive a general framework to more clearly extract how slowly the diffusive regime is approached. Let  $\rho(\mathbf{r}, t)$  be the bacterial density at vector position  $\mathbf{r}$  at time  $t$  obtained by averaging over different realizations. The initial condition is such that a single bacterium is located at the origin,  $\rho(\mathbf{r}, 0) = \delta(\mathbf{r})$ , but its orientation and internal state are otherwise random. With this initial condition,  $\rho$  is called also the van Hove function [25]. The MSD is

$$\langle r^2(t) \rangle = \int d\mathbf{r} r^2 \rho(\mathbf{r}, t). \quad (1)$$

When at long times the diffusive regime is achieved,  $\langle r^2(t) \rangle \sim t$  and the diffusion coefficient is obtained with the Einstein relation [26],

$$D = \lim_{t \rightarrow \infty} \frac{\langle r^2(t) \rangle}{4t}, \quad (2)$$

in two spatial dimensions. Calculations become easier to perform through the definition of

$$\tilde{\rho}(\mathbf{k}, s) \equiv \int_0^\infty dt e^{-st} \int d\mathbf{r} e^{-i\mathbf{k}\cdot\mathbf{r}} \rho(\mathbf{r}, t) \quad (3)$$

as the Laplace–Fourier transform of  $\rho(\mathbf{r}, t)$ , where  $\mathbf{k}$  is the Fourier wave vector and  $s$  is the Laplace complex variable.

Similarly to what is derived in Ref. [25], the second spatial moment (MSD) and the fourth spatial moment in 2D can be calculated, respectively, from

$$\langle r^2(t) \rangle = \mathcal{L}^{-1} \left\{ -2 \frac{\partial^2}{\partial k^2} \tilde{\rho}(\mathbf{k}, s) \Big|_{k=0} \right\} \quad (4)$$

and

$$\langle r^4(t) \rangle = \mathcal{L}^{-1} \left\{ \frac{8}{3} \frac{\partial^4}{\partial k^4} \tilde{\rho}(\mathbf{k}, s) \Big|_{k=0} \right\}, \quad (5)$$

where  $\mathcal{L}^{-1}$  denotes the inverse Laplace transform operator used to bring the result back to the time  $t$  domain. The corresponding diffusion coefficient  $D$  can be expressed as [25]

$$D = \lim_{\omega \rightarrow 0} \lim_{k \rightarrow 0} \frac{\omega^2}{k^2} \text{Re} [\tilde{\rho}(\mathbf{k}, i\omega)], \quad (6)$$

where  $\omega$  is real,  $k \equiv |\mathbf{k}|$ , and  $\text{Re}(\tilde{\rho})$  denotes the real part of  $\tilde{\rho}$ . In order to measure the non-Gaussianity of a particle's displacement distribution we will be interested in the excess kurtosis, defined in 2D by

$$\gamma(t) \equiv \frac{\langle r^4 \rangle}{\langle r^2 \rangle^2} - 2. \quad (7)$$

The excess kurtosis is dimensionless and vanishes for a Gaussian distribution of displacements.

### A. Extracting the excess kurtosis tail

In general, we will see that  $\langle r^2 \rangle$  and  $\langle r^4 \rangle$  approach their asymptotic regimes with exponential and subdominant polynomial corrections. As a result, the excess kurtosis approaches zero as

$$\gamma(t) \sim \sum_n a_n t^{-\beta_n} e^{-\mu_n t}, \quad (8)$$

with particular sets of coefficients  $a_n$ , exponents  $\beta_n \geq 0$ , and rates  $\mu_n \geq 0$  that depend on the model under consideration. We are looking for the slow decay modes to the diffusive regime, which can appear when  $\mu_n$  are close to zero and  $\beta_n$  are small. From the definition (7), exponential factors can appear either in the second or fourth moment. For example, for the second moment,

$$\langle r^2(t) \rangle \sim 4Dt + \sum_{n=0}^{\infty} c_n t^{\gamma_n} e^{-\mu_n t}, \quad (9)$$

which in Laplace space gives for small  $s$

$$\langle \tilde{r}^2(s) \rangle \sim \frac{4D}{s^2} + \sum_{n=0}^{\infty} \frac{c_n \gamma_n!}{(s + \mu_n)^{1+\gamma_n}} \quad (10)$$

and similarly for  $\langle \tilde{r}^4(s) \rangle$ . Hence, the exponents  $\mu_n$  are recognized as minus the poles of  $\partial_k^2 \tilde{\rho}(\mathbf{k}, s)|_{k=0}$  and  $\partial_k^4 \tilde{\rho}(\mathbf{k}, s)|_{k=0}$ . The slowest decaying mode will be identified as the smallest positive  $\mu_n$ . For the majority of the models considered in this article, the long-time behavior of excess kurtosis can be explicitly obtained in real time. However, for the last model, we will need to extract it from Laplace space, as there is no closed expression for  $\gamma(t)$ .

### III. CONSTANT TUMBLING RATE

We will now examine three separate limiting cases of the well known Markovian run-and-tumble model. Consider a particle moving in two spatial dimensions, for which tumbling occurs at a constant rate  $\nu_0$ . That is, the random walker moves with a constant speed  $V$  along a body-axis  $\hat{\mathbf{n}} = (\cos\theta, \sin\theta)$  that can change abruptly at a tumble event, suddenly decorrelating its orientation—in the case of *E. coli* the duration of the tumble is about ten times smaller than the duration of the runs [10] and so it is taken as zero here. The new random orientation is chosen with a kernel  $W(\theta, \theta')$  that sets the probability that the swimmer changes between two specified orientation angles  $\theta$  and  $\theta'$  at a tumble. We will assume that the space is isotropic, hence, the kernel only depends on the angle difference,  $W(\theta, \theta') = w(\theta_s)$ , where  $w$  is an even periodic function and  $\theta_s \equiv \theta' - \theta$  is the tumbling angle. In addition to that, the model's particle is subject to thermal rotational diffusion with coefficient  $D_r$ . Thus, in the meantime between two consecutive tumbles the orientation will change slowly and diffusively. The kinetic equation for the distribution function  $f = f(\mathbf{r}, \theta, t)$  is [22–24, 27]

$$\frac{\partial f}{\partial t} + V\hat{\mathbf{n}} \cdot \nabla f = \nu_0 \int_0^{2\pi} w(\theta' - \theta) f(\mathbf{r}, \theta', t) d\theta' - \nu_0 f + D_r \nabla_{\hat{\mathbf{n}}}^2 f, \quad (11)$$

where the distribution function is normalized such that  $\rho(\mathbf{r}, t) = \int_0^{2\pi} f(\mathbf{r}, \theta, t) d\theta$ . The kernel satisfies  $\int w(\theta) d\theta = 1$ , which guarantees that the density  $\rho$  is conserved.

#### A. Conventional run-and-tumble model

We start with the limiting case where  $D_r = 0$  and there is complete reorientation after tumbling, that is,  $w(\theta_s) = 1/2\pi$ , the simplest version of the run-and-tumble model. This will serve to calibrate our methodology. In this case the kinetic equation for the probability density function  $f(\mathbf{r}, \theta, t)$  is just

$$\frac{\partial f}{\partial t} + V\hat{\mathbf{n}} \cdot \nabla f = \frac{\nu_0}{2\pi} \int_0^{2\pi} f(\mathbf{r}, \theta', t) d\theta' - \nu_0 f. \quad (12)$$

The initial condition is  $f(\mathbf{r}, \theta, 0) = \delta(\mathbf{r})/2\pi$ , meaning that the initial orientation is random. With a view to obtaining  $\tilde{\rho}(\mathbf{k}, s)$  satisfying this kinetic equation, we move to Laplace–Fourier space. This leads to Eq. (12) being rewritten as

$$(s + iV\mathbf{k} \cdot \hat{\mathbf{n}} + \nu_0) \tilde{f} = \frac{1}{2\pi} (1 + \nu_0 \tilde{\rho}), \quad (13)$$

where we used that

$$\tilde{\rho}(\mathbf{k}, s) = \int_0^{2\pi} \tilde{f}(\mathbf{k}, \theta, s) d\theta \quad (14)$$

for the Laplace–Fourier transform  $\tilde{f}(\mathbf{k}, \theta, s)$  of the distribution function. Therefore by isolating  $\tilde{f}(\mathbf{k}, \theta, s)$  and integrating over  $\theta$  we obtain a closed equation for  $\tilde{\rho}$ , which gives

$$\begin{aligned} \tilde{\rho}(\mathbf{k}, s) &= \frac{1}{\sqrt{(s + \nu_0)^2 + V^2 k^2} - \nu_0}, \\ &= \frac{1}{s} - \frac{V^2 k^2}{2s^2(s + \nu_0)} + \frac{(3s + 2\nu_0)V^4 k^4}{8s^3(s + \nu_0)^3} + \mathcal{O}(k^6), \end{aligned} \quad (15)$$

where in the second line we made a Taylor expansion in  $k$  to easily identify the poles associated to the second and fourth moments. We can now use the equations in Section II to obtain our desired quantities. The MSD is

$$\langle r^2 \rangle = \frac{2V^2}{\nu_0^2} (\nu_0 t + e^{-\nu_0 t} - 1), \quad (17)$$

from which one can either use Einstein relation (2) or directly apply Eq. (6) to obtain

$$D = \frac{V^2}{2\nu_0}, \quad (18)$$

which is a widely known result [28–30]. The fourth spatial moment reads

$$\langle r^4 \rangle = \frac{4V^4}{\nu_0^4} [2(\nu_0^2 t^2 - 3\nu_0 t + 3) + e^{-\nu_0 t}(\nu_0^2 t^2 - 6)], \quad (19)$$

allowing to compute directly the excess kurtosis. The kurtosis longest-standing exponential goes as  $\exp(-\nu_0 t)$ , which does not present any singular behavior.

In Fig. 1 the above expressions for the MSD, the diffusion coefficient, and the excess kurtosis are tested against our simulations, which have been performed by directly solving the associated run-and-tumble motion equations. The agreement is excellent as expected since no approximations were made.

#### B. Partial reorientation

We now generalize the previous analysis to the case of partial reorientation while keeping  $D_r = 0$ . In this case the kernel is no longer uniformly distributed between 0 and  $2\pi$ . The tumbling kernel is fully characterized by its cosine Fourier components

$$\sigma_n \equiv \langle \cos(n\theta_s) \rangle = \int_{-\pi}^{\pi} d\theta_s w(\theta_s) \cos(n\theta_s), \quad n \geq 1, \quad (20)$$

which, in the previous case, vanish completely. It can be shown that the mean-squared displacement depends on  $\sigma_1$  only [5]. Thus, for that purpose, only the average value  $\sigma_1$  matters and so we do not need to worry about the whole shape of  $w$ . However, we show below that

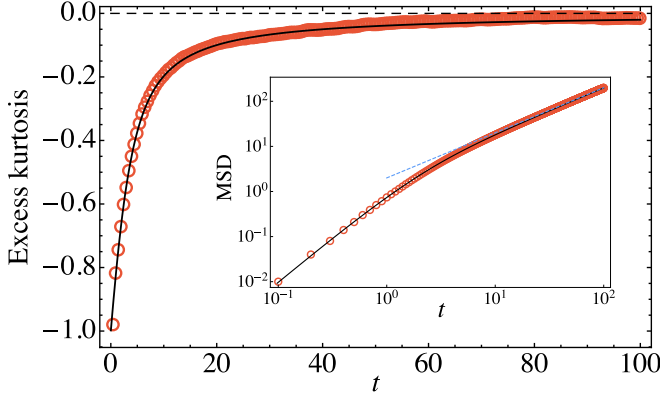


FIG. 1. Conventional run-and-tumble model: theory (solid black line) and simulation (circles) for the time evolution of the excess kurtosis and, in the inset, of the MSD (log-log scale). The dashed line is  $4Dt$  where the diffusion coefficient  $D$  is given by Eq. (18). Units are chosen such that  $V = \nu_0 = 1$ .

the excess kurtosis and the crossover time to reach the diffusive regime depend also on  $\sigma_2$ .

The Laplace–Fourier transform of the kinetic equation (11) for this case is

$$(s + iV\mathbf{k} \cdot \hat{\mathbf{n}} + \nu_0) \tilde{f} = \frac{1}{2\pi} + \nu_0 \int_0^{2\pi} w(\theta' - \theta) \tilde{f}(\mathbf{k}, \theta', s) d\theta', \quad (21)$$

where we used the same initial condition as in Sect. III A. To solve it, we expand the distribution function in Fourier modes

$$\tilde{f}(\mathbf{k}, \theta, s) = \sum_{n=0}^{\infty} [h_n \cos(n\theta) + g_n \sin(n\theta)], \quad (22)$$

where the coefficients  $h_n$  and  $g_n$  depend on  $\mathbf{k}$  and  $s$ , and are to be determined by plugging the solution into the kinetic equation. Taking  $\mathbf{k} = k\hat{\mathbf{x}}$ , it is clear that the sine modes will vanish identically, and so we can set  $g_n = 0$  from now on. As  $w$  is even, the integral is a convolution that can be expressed as

$$\int_0^{2\pi} w(\theta' - \theta) \tilde{f}(\mathbf{k}, \theta', s) d\theta' = \sum_{n=0}^{\infty} \sigma_n h_n \cos(n\theta). \quad (23)$$

By keeping terms up to  $n = 2$ , we truncate the Fourier series, which allows us to obtain a closed expression for  $\tilde{\rho}(\mathbf{k}, s)$ . For the sake of presentation the long result is expressed as an expansion up to fourth order in  $k$ . This has no implications as no higher-order derivative in  $k$  will be required. We have

$$\tilde{\rho}(\mathbf{k}, s) = \frac{1}{s} - \frac{V^2 k^2}{2s^2 (\nu_0(1 - \sigma_1) + s)} + \frac{(3s - 2\nu_0(\sigma_2 - 1)) V^4 k^4}{8s^3 (\nu_0(1 - \sigma_1) + s)^2 (\nu_0(1 - \sigma_2) + s)} + \mathcal{O}(k^6). \quad (24)$$

Using the expressions of Sect. II, the MSD is

$$\langle r^2 \rangle = \frac{2V^2}{\nu_0^2(1 - \sigma_1)} \left[ \nu_0 t + \frac{e^{-\nu_0(1 - \sigma_1)t} - 1}{(1 - \sigma_1)} \right], \quad (25)$$

with diffusion coefficient

$$D = \frac{V^2}{2\nu_0(1 - \sigma_1)}, \quad (26)$$

which is a well known result [24, 27]. The fourth moment is

$$\langle r^4 \rangle = \frac{8V^4}{\nu_0^4} \left[ \frac{\nu_0^2 t^2}{(1 - \sigma_1)^2} + \frac{e^{-\nu_0(1 - \sigma_2)t}}{(\sigma_1 - \sigma_2)^2 (1 - \sigma_2)^2} - \frac{\sigma_1^2 + 2(\sigma_2 - 2)\sigma_1 - 6\sigma_2^2 + 10\sigma_2 - 3}{(1 - \sigma_1)^4 (1 - \sigma_2)^2} - \frac{\nu_0(3\sigma_1 - 2\sigma_2 - 1)te^{-\nu_0(1 - \sigma_1)t}}{(1 - \sigma_1)^3 (\sigma_1 - \sigma_2)} + \frac{\nu_0(\sigma_1 - 4\sigma_2 + 3)t}{(1 - \sigma_1)^3 (\sigma_2 - 1)} - \frac{(9\sigma_1^2 - 2(7\sigma_2 + 2)\sigma_1 + 6\sigma_2^2 + 2\sigma_2 + 1)e^{-\nu_0(1 - \sigma_1)t}}{(1 - \sigma_1)^4 (\sigma_1 - \sigma_2)^2} \right]. \quad (27)$$

While for the complete-reorientation kernel of Sect. III A there is a single relaxation time, for a general kernel two relaxation rates appear:  $\nu_1 = \nu_0(1 - \sigma_1)$  and  $\nu_2 = \nu_0(1 - \sigma_2)$ . In this regard, the complete-reorientation case is singular since the two relaxation times merge, increasing the multiplicity of the corresponding pole in (24). This implies that, while for the complete-reorientation case the excess kurtosis decay purely exponentially as  $\gamma \sim \exp(-\nu_0 t)$ , here it will be as  $\gamma \sim \exp(-\nu_1 t)/t$  and  $\gamma \sim \exp(-\nu_2 t)/t^2$ , except for the singular case where both rates are equal, in which  $\gamma \sim \exp(-\nu_1, 2t)$ .

The approach to a linear time dependence in the MSD is controlled by  $\nu_1$ . The corresponding relaxation time diverges when  $\sigma_1 \approx 1$ , which happens if the average tumbling angle is small. Naturally, in this case, when swimmers deviate little in each tumble event the persistence is enhanced, implying a large diffusion coefficient. Importantly, also the amplitude of the non-diffusive term diverges when  $\sigma_1 \approx 1$ , making such a departure from diffusion more relevant.

The second rate appears in the fourth moment given by Eq. (27). Both the relaxation time and the associated amplitude diverge when  $\sigma_2 \approx 1$ , implying that for long times the displacement distribution deviates largely from a Gaussian one. If, simultaneously,  $\sigma_1$  is far from one, then although the MSD reaches the linear regime rapidly, the excess kurtosis remains finite for long times. This situation can occur, for example, if the tumbling angles distribution is sharply centered around both 0 and  $180^\circ$ . Then, for a single swimmer, the tumbles give rise to a one-dimensional random walk along  $\hat{\mathbf{n}}$  and only slowly, with a rate proportional to the dispersion of tumbling angles around 0 and  $\pi$ , i.e.,  $\sigma_2$ , the process evolves to a two-dimensional diffusion. For a collection of swimmers

initially seeded at  $\mathbf{r} = 0$ , the intermediate dynamics for  $T_1 < t < T_2$  will be diffusive only in the radial direction. We recall that a mean-squared displacement that grows linearly with time is a necessary but not sufficient condition to have diffusion. It is also necessary that the displacements follow a Gaussian distribution.

In order to compare to simulations, we now need to specify a kernel  $w$ . Two cases are considered. First, we take the tumbling angles uniformly distributed in the range  $[-\Delta/2, \Delta/2]$ , in which case  $T_1$  and  $T_2$  are of similar order. The second case is for  $\theta_s$  uniformly distributed in the ranges  $[-\Delta/4, \Delta/4]$  and  $[180^\circ - \Delta/4, 180^\circ + \Delta/4]$  where for small  $\Delta$  there is a strong separation of time scales. Figure 2 shows that our numerical results and the theory agree well despite the approximation made in truncating the Fourier series up to  $n = 2$ . The smaller the  $\Delta$  the longer it takes to reach the diffusive regime since the motion gets more ballistic. Note particularly that in the second case, when  $\Delta$  is small, the displacement distributions remain largely non-Gaussian even when the mean-squared displacements grow linearly.

### C. Run-and-reverse with thermal rotational diffusion

In the limiting case known as run-and-reverse dynamics the particle's tumble can only lead to the exactly opposite motion direction. In this limit it becomes physically unreasonable to neglect thermal diffusion and so we will take  $D_r \neq 0$ ; otherwise the swimmer will indefinitely perform a one-dimensional random walk. In this model  $w(\theta_s) = \delta(\theta_s - \pi)$ , and hence the kinetic equation reads

$$\frac{\partial f}{\partial t} + V \hat{\mathbf{n}} \cdot \nabla f = \nu_0 f(\mathbf{r}, \theta + \pi, t) - \nu_0 f + D_r \frac{\partial^2 f}{\partial \theta^2}, \quad (28)$$

where we notice that the indicated instance of  $f$  is evaluated at  $\theta + \pi$ , while the other ones are evaluated at  $\theta$  as per usual. After the Laplace–Fourier transform is applied and using the same initial condition as before, i.e.,  $f(\mathbf{r}, \theta, 0) = \delta(\mathbf{r})/2\pi$ , we obtain

$$(s + iV\mathbf{k} \cdot \hat{\mathbf{n}} + \nu_0) \tilde{f} - \nu_0 \tilde{f}(\mathbf{k}, \theta + \pi, s) - D_r \frac{\partial^2 \tilde{f}}{\partial \theta^2} = \frac{1}{2\pi}. \quad (29)$$

Similarly to the previous case we expand  $\tilde{f}$  in a Fourier series (22), where again  $g_n = 0$  by symmetry. We truncate the series keeping only the terms  $n \leq 2$  and solve for the coefficients. Integrating  $\tilde{f}(\mathbf{k}, \theta, s)$  over  $\theta$ , we obtain

$$\tilde{\rho}(\mathbf{k}, s) = \frac{4(4D_r + s)(D_r + 2\nu_0 + s) + V^2 k^2}{8V^2 k^2 D_r + 20D_r s^2 + 8\nu_0 s(4D_r + s) + 16sD_r^2 + 3sV^2 k^2 + 4s^3}. \quad (30)$$

Upon using the formulae in Section II, we find that the MSD is given by

$$\langle r^2 \rangle = \frac{2V^2}{(D_r + 2\nu_0)^2} \left[ (D_r + 2\nu_0)t + e^{-(D_r + 2\nu_0)t} - 1 \right], \quad (31)$$

with diffusion coefficient

$$D = \frac{V^2}{2(D_r + 2\nu_0)}, \quad (32)$$

while the fourth moment is

$$\langle r^4 \rangle = \frac{V^4}{2} \left[ \frac{87D_r^2 - 4\nu_0^2 - 20\nu_0 D_r}{D_r^2 (D_r + 2\nu_0)^4} + \frac{16t^2}{(D_r + 2\nu_0)^2} + \frac{8\nu_0 t - 60D_r t}{D_r (D_r + 2\nu_0)^3} + \frac{e^{-4D_r t}}{D_r^2 (3D_r - 2\nu_0)^2} \right. \\ \left. - \frac{16e^{-(D_r + 2\nu_0)t} (D_r^2 (2\nu_0 t + 49) - 4\nu_0 D_r (11\nu_0 t + 19) + 15D_r^3 t + 12\nu_0^2 (2\nu_0 t + 3))}{(3D_r - 2\nu_0)^2 (D_r + 2\nu_0)^4} \right]. \quad (33)$$

As in the previous case and for analogous reasons, the MSD can reach rapidly a regime where it grows linearly with time, but for small rotational diffusion, the process remains non Gaussian. The diffusive regime is only

achieved at a time scale  $1/(4D_r)$ .

For small enough rotational diffusion, the excess kurtosis becomes positive, presenting a peak that can be quite large (see Fig. 3). This implies that the displacement

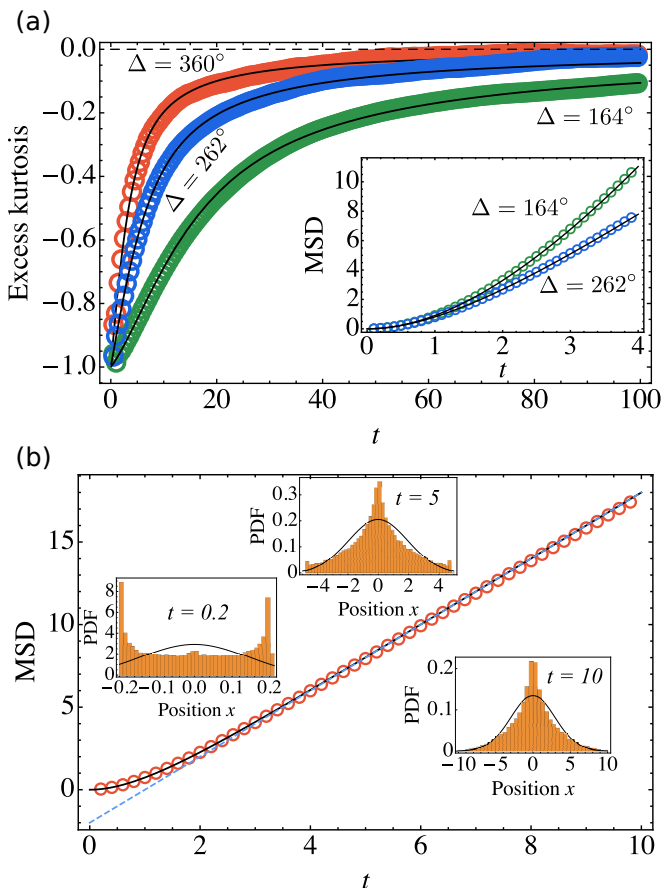


FIG. 2. Run-and-tumble model with partial reorientation. Top: theory (solid black lines) and simulation (circles) for the excess kurtosis as a function of time (and for the MSD in the inset). The values of  $\Delta$  are indicated in degrees:  $164^\circ$ ,  $262^\circ$ , and, the complete-reorientation limit,  $360^\circ$  (green, blue, and red, respectively). Bottom: MSD for a kernel uniformly distributed around both  $0^\circ$  and  $180^\circ$  with  $\Delta = 20^\circ$  as re-defined in the main text. Theory (solid black line), simulation (circles), and the linear part of the MSD (dashed blue line). Insets: probability distribution function of the  $x$ -displacement at different time instants as from simulations (solid lines are normalized Gaussian distributions with the same mean and variance as the corresponding data). Units are chosen such that  $V = \nu_0 = 1$ .

distribution presents large tails. Positive kurtosis with a very slow decay also appear in the similar of partial reorientation without rotational diffusion (Sect. III B) for  $\sigma_2 \approx 1$ , as can be seen directly from Eq. (27).

#### IV. STOCHASTIC TUMBLING RATE

In bacteria like *E. coli*, the tumbling process is triggered by a reversion in the sense of rotation (from counter-clockwise, CCW, to clockwise, CW) of one or several flagella. As a result, the flagella bundle disassembles and the propulsion thrust is lost [31]. By analyzing the biochemistry of the molecular motor, Tu and

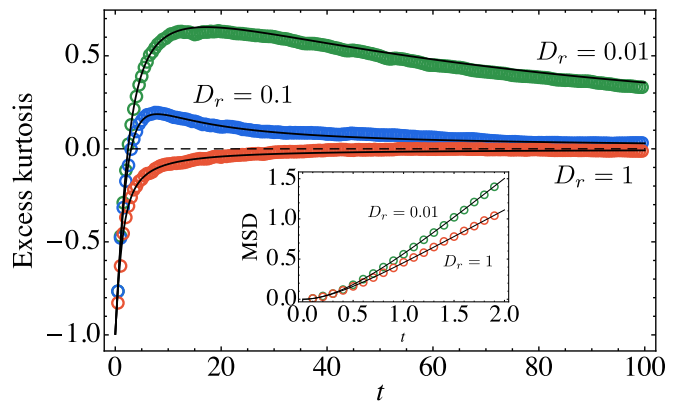


FIG. 3. Run-and-reverse model with rotational diffusion: theory (solid black lines) and simulation (circles) for the excess kurtosis as a function of time (and for the MSD in the inset). The values of  $D_r$  are indicated:  $0.01$ ,  $0.1$ , and  $1$  (green, blue, and red, respectively). Units are chosen such that  $V = \nu_0 = 1$ .

Grinstein proposed that the tumbling process can be described as a two state activated system, where the free energy barrier to transit from the CCW to the CW state depends sensibly on the concentration inside the bacterial body of the so-called CheY-P protein, denoted by  $[Y]$  [14]. In the Tu-Grinstein model the tumble rate is  $\nu = \bar{\nu} \exp(-G([Y])/k_B T)$ , where  $G$  is the free energy barrier and  $\bar{\nu}$  a constant. Expanding  $G$  around the average value  $[Y_0]$ , they propose

$$\nu(X) = \nu_0 e^{\alpha X}, \quad (34)$$

where  $X(t) = ([Y](t) - [Y_0])/\sigma_Y$  corresponds to the fluctuations in concentration normalized to  $\sigma_Y$ , the standard deviation of  $[Y]$ , and  $\nu_0$  absorbs all the prefactors. The parameter  $\alpha$  is positive [32] and quantifies the sensitivity of the system to changes in the protein concentration. This phosphorylated protein has a small production rate, with a long memory time  $T$ , and consequently  $X$  is well described by the Ornstein-Uhlenbeck process

$$\frac{dX}{dt} = -\frac{X}{T} + \sqrt{\frac{2}{T}}\xi(t), \quad (35)$$

where  $\xi$  is an additive zero-mean Gaussian white noise with correlation  $\langle \xi(t)\xi(t') \rangle = \delta(t-t')$ . By tracking individual *E. coli* bacteria it has been possible to fit the model parameters to  $T = 19.0$  s,  $\nu_0 = 0.65$  s $^{-1}$ , and  $\alpha = 1.62$  [33]. The same experiments gave for the rotational diffusivity  $D_r = 0.025$  s $^{-1}$  and for the tumbling  $\sigma_1 = 0.112$ . Considering that  $D_r \ll \nu_0$  and that  $\sigma_1 \approx 0$ , we will consider complete reorientation after tumbling and neglect the rotational diffusion. This approximation also helps to highlight the new phenomenology that appears from considering the internal variable  $X$ .

With  $X$  as a new variable of the distribution function,

the kinetic equation for  $f = f(\mathbf{r}, \theta, X, t)$  reads

$$\begin{aligned} \frac{\partial f}{\partial t} + V \hat{\mathbf{n}} \cdot \nabla f &= \frac{1}{T} \left[ \frac{\partial^2 f}{\partial X^2} + \frac{\partial(Xf)}{\partial X} \right] \\ &+ \frac{\nu(X)}{2\pi} \int_0^{2\pi} f(\mathbf{r}, \theta', X, t) d\theta' - \nu(X)f. \end{aligned} \quad (36)$$

where the distribution function is normalized such that  $\rho(\mathbf{r}, t) = \int f(\mathbf{r}, \theta, X, t) d\theta dX$ .

Once again, we change to the Laplace–Fourier space and so Eq. (36) becomes

$$\begin{aligned} s\tilde{f} - \frac{1}{(2\pi)^{3/2}} e^{-X^2/2} + iV\mathbf{k} \cdot \hat{\mathbf{n}}\tilde{f} &= \\ \frac{1}{T} \left[ \frac{\partial^2 \tilde{f}}{\partial X^2} + \frac{\partial(X\tilde{f})}{\partial X} \right] + \nu(X) \left[ \frac{\tilde{g}(\mathbf{k}, X, s)}{2\pi} - \tilde{f} \right], \end{aligned} \quad (37)$$

where  $\tilde{f}$  stands for  $\tilde{f}(\mathbf{k}, \theta, X, s)$ , and we have made use of the definition

$$\tilde{g}(\mathbf{k}, X, s) \equiv \int_0^{2\pi} \tilde{f}(\mathbf{k}, \theta', X, s) d\theta' \quad (38)$$

and the initial condition

$$f(\mathbf{r}, \theta, X, t = 0) = \frac{1}{(2\pi)^{3/2}} e^{-X^2/2} \delta(\mathbf{r}), \quad (39)$$

which indicates that the internal variable  $X$  is in equilibrium. We propose the solution

$$\tilde{f}(\mathbf{k}, \theta, X, s) = \sum_{n=0}^{\infty} G_n(X) \tilde{f}_n(\mathbf{k}, \theta, s), \quad (40)$$

where the coefficients  $\tilde{f}_n(\mathbf{k}, \theta, s)$  do not depend on  $X$  and

$$G_n(X) \equiv e^{-X^2/2} H_n(X/\sqrt{2}), \quad (41)$$

in which  $H_n$  denotes the so-called physicists' Hermite polynomial of order  $n$  [such that  $H_0(x) = 1$ ,  $H_1(x) = 2x$ , ...] [34]. Using the eigenvalue equation for the Hermite polynomials allows us to write

$$\begin{aligned} \frac{1}{T} \left[ \frac{\partial^2 \tilde{f}(\mathbf{k}, \theta, X, s)}{\partial X^2} + \frac{\partial(X\tilde{f}(\mathbf{k}, \theta, X, s))}{\partial X} \right] &= \\ -\frac{1}{T} \sum_{n=0}^{\infty} n e^{-X^2/2} H_n(X/\sqrt{2}) \tilde{f}_n(\mathbf{k}, \theta, s). \end{aligned} \quad (42)$$

Since our goal is to find the Laplace–Fourier transform of  $\rho(\mathbf{r}, t)$ , i.e.,  $\tilde{\rho}(\mathbf{k}, s)$ , which does not depend on  $\theta$ , it is helpful to define  $\tilde{g}_n(\mathbf{k}, s) = \int_0^{2\pi} \tilde{f}_n(\mathbf{k}, \theta, s) d\theta$ .

At this point we proceed by plugging the above equations into Eq. (37), then multiplying by  $H_m(X/\sqrt{2})$ , and finally integrating over  $X$ . One obtains

$$\sum_{n=0}^{\infty} A_{mn}(\mathbf{k}, \theta, s) \tilde{f}_n(\mathbf{k}, \theta, s) = c_m + \sum_{n=0}^{\infty} B_{mn} \tilde{g}_n(\mathbf{k}, s), \quad (43)$$

where

$$A_{mn}(\mathbf{k}, \theta, s) \equiv 2^n n! \sqrt{\pi} \delta_{mn} \left( s + iV\mathbf{k} \cdot \hat{\mathbf{n}} + \frac{n}{T} \right) + \nu_0 J_{mn}, \quad (44)$$

$$B_{mn} \equiv \frac{\nu_0}{2\pi} J_{mn}, \quad c_m \equiv \frac{1}{2\pi\sqrt{2}} \delta_{m0}, \quad (45)$$

where the  $\delta_{ij}$  are Kronecker deltas and

$$J_{mn} \equiv \int_{-\infty}^{\infty} e^{-y^2} e^{\sqrt{2}\alpha y} H_n(y) H_m(y) dy. \quad (46)$$

The linear Eqs. (43) can be solved for  $\tilde{f}_n$  in terms of  $\tilde{g}_n$ . Integrating over  $\theta$  gives now a closed linear set of equations for  $\tilde{g}_n$ , which can be directly solved. Noting that  $\tilde{\rho} = \tilde{g}_0$  (which can be seen through the orthogonality between  $H_0$  and  $H_n$ ), one obtains

$$\begin{aligned} \tilde{\rho}(\mathbf{k}, s) &= \int_0^{2\pi} \left[ \frac{1}{2\sqrt{\pi}} (\mathbf{A}^{-1})_{00}(\mathbf{k}, \theta, s) \right. \\ &\left. + \sqrt{2\pi} \sum_{m,n=0}^{\infty} (\mathbf{A}^{-1})_{0m}(\mathbf{k}, \theta, s) B_{mn} \tilde{g}_n(\mathbf{k}, s) \right] d\theta. \end{aligned} \quad (47)$$

To obtain explicit expressions, Eq. (47) is truncated at a certain order  $n = m = N_{\max}$ . The greater the  $N_{\max}$  the higher is the order of a polynomial in  $\alpha$  that appears in  $J_{mn}$ . Hence, increasing  $N_{\max}$  one increases the range in  $\alpha$  over which the theory is valid. However, the greater the  $N_{\max}$  the more complicated are the elements of the inverse of  $\mathbf{A}$ , which eventually need to be integrated in  $\theta$ . Therefore  $N_{\max}$  also affects how complicated it is the  $\tilde{\rho}(\mathbf{k}, s)$  over which one needs to apply the inverse Laplace transform as well as to compute limits. As it turns out, those complications grow rapidly with  $N_{\max}$ , with the case  $N_{\max} = 0$  being the only one that we have treated fully analytically. The  $\tilde{\rho}(\mathbf{k}, s)$  obtained by expanding up to this order is identical to the conventional RT case (15), provided that one considers the tumbling rate to be  $\nu_0 \exp(\alpha^2/2)$ , which corresponds to the average of Eq. (34) over  $X$ . See Section IV A for the related analysis of the limits  $T \rightarrow 0$  and  $T \rightarrow \infty$ .

For  $N_{\max} = 1$  new physics is found. Although involved, it is possible to obtain an explicit expression for  $\tilde{\rho}(\mathbf{k}, s)$  from where the diffusion coefficient is obtained using Eq. (6),

$$D = \frac{V^2}{2\nu_0 e^{\alpha^2/2}} \left( 1 + \frac{\alpha^2 \nu_0 T}{1 + \nu_0 T} \right). \quad (48)$$

It is not possible, however, to analytically perform the inverse transforms of the second and fourth moments. Instead, they are calculated by applying a semi-numerical inverse Laplace transform method for comparison with simulations. As one can see in Fig. 4, the analytical results in this case agree very well with simulations up to a significant value of  $\alpha$ .

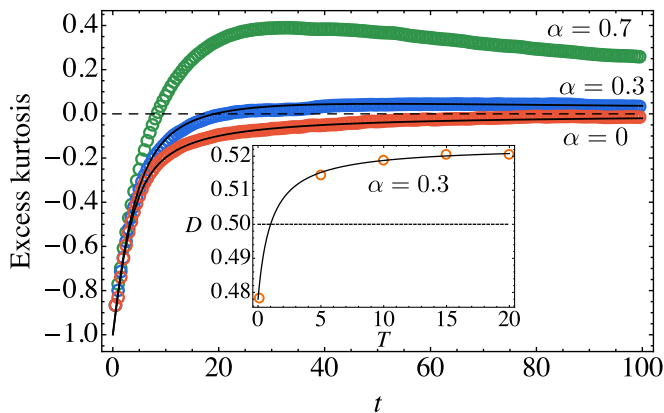


FIG. 4. Run-and-tumble model with stochastic tumbling rate: theory (solid black lines) and simulation (circles) for the excess kurtosis as a function of time for  $T = 20$ . It shows the cases  $\alpha = 0.3$  and the conventional RT limit  $\alpha = 0$  (blue and red, respectively). Simulation data for  $\alpha = 0.7$  is shown (in green) without the small- $\alpha$  theory. Inset: theoretical prediction [Eq. (54)] and simulation for the diffusion coefficient  $D$  vs. the protein memory  $T$  (see main text). The horizontal dashed line shows the conventional RT prediction  $D = 1/2$  as a reference. Units are chosen such that  $V = \nu_0 = 1$ .

Despite the aforementioned complications in obtaining an expression for  $\tilde{\rho}(\mathbf{k}, s)$ , we can still use the method in Section II A to extract the late-time exponential decay of the excess kurtosis. The second and fourth moments share poles, and upon reversing their sign we obtain

$$\nu_1 = \nu_0[1 + \alpha^2(1/2 - T\nu_0) + \mathcal{O}(\alpha^4)], \quad (49)$$

$$\nu_2 = \nu_0[1 + 1/(T\nu_0) + \alpha^2(3/2 + T\nu_0) + \mathcal{O}(\alpha^4)]. \quad (50)$$

While the second rate remains finite for all values of the parameters,  $\nu_1$  decays linearly with  $T$ . Therefore the greater the protein memory the longer it will take for diffusion to be achieved. But the behavior for varying  $\alpha$  depends on where in the memory  $T$  range we are: if  $T\nu_0 > 1/2$  then  $\nu_1$  also decays with  $\alpha$ , meaning a slower approach to diffusion, and if  $T\nu_0$  is smaller than that then increasing  $\alpha$  speeds up the approach. To evaluate the importance of this eventual slow approach to diffusion, we compute the multiplicity and amplitude of the associated pole, obtaining

$$\langle \tilde{r}^4(s) \rangle \sim \frac{8V^4[1 + \nu_0 T(1 + 2\nu_0 T)\alpha^2/2 + \mathcal{O}(\alpha^4)]}{\nu_0^2(s + \nu_1)^3} \quad (51)$$

This implies that at long times the kurtosis exponential decay is  $\gamma \sim \exp(-\nu_1 t)$ , with an amplitude that grows with  $\alpha$ , in agreement with the results shown in Fig. 4.

### A. Zero- and infinite-memory limits

In the limiting case of very small memory time  $T$ ,  $X$  fluctuates rapidly and the tumble rate is effectively an

average of (34) over all possible values of  $X$ , that is,  $\langle \nu \rangle = \nu_0 \exp(\alpha^2/2)$ . This result can be achieved more formally by expanding the distribution function  $\tilde{f}$  for small  $T$  as  $\tilde{f} = f_0 + T\tilde{f}_1 + \mathcal{O}(T^2)$  and  $\tilde{g} = \tilde{g}_0 + T\tilde{g}_1 + \mathcal{O}(T^2)$ , and replacing these into the Laplace-Fourier-transformed kinetic equation (37). For  $\mathcal{O}(1/T)$  we obtain a simple differential equation in  $X$  for  $\tilde{f}_0$  whose solution can be cast as  $\tilde{f}_0 = e^{-X^2/2} a(\mathbf{k}, \theta, s)$  where  $a(\mathbf{k}, \theta, s)$  is some coefficient function independent of  $X$ . At  $\mathcal{O}(T)$  the equation reads

$$iV\mathbf{k} \cdot \hat{\mathbf{n}} e^{-X^2/2} a + s e^{-X^2/2} a + \nu_0 e^{-X^2/2 + \alpha X} a - \frac{\nu_0 e^{-X^2/2 + \alpha X} b}{\sqrt{2\pi}} - \frac{e^{-X^2/2}}{(2\pi)^{3/2}} = \frac{\partial^2 \tilde{f}_1}{\partial X^2} + \frac{\partial(X\tilde{f}_1)}{\partial X}, \quad (52)$$

where  $b(\mathbf{k}, s) \equiv \int_0^{2\pi} a(\mathbf{k}, \theta, s) d\theta$ . The RHS can be viewed as a differential operator  $\mathcal{D}$  acting on  $\tilde{f}_1$ , where the kernel of the adjoint operator  $\mathcal{D}^\dagger$  is 1. Thus, upon using the Fredholm Alternative theorem, setting the  $X$ -integral of the LHS to zero, one gets the conventional RT equation (12) with tumbling rate  $\langle \nu \rangle$ . Therefore,  $D_{T \rightarrow 0} = V^2/[2\nu_0 \exp(\alpha^2/2)]$ , as previously anticipated.

The  $T \rightarrow \infty$  limit is also interesting. In this case a particle starts with a certain protein concentration (and hence a certain tumbling rate) as determined by  $X$ , which is then kept fixed at all times. The system is therefore equivalent to considering a ‘‘polydisperse dilute fluid’’, that is, a set of non-interacting particles, where each one has a fixed tumbling rate  $\nu_i$  drawn from a continuous distribution. Thus the averaged diffusion coefficient is

$$D_{T \rightarrow \infty} = \left\langle \frac{V^2}{2\nu_i} \right\rangle = \frac{V^2}{2\nu_0} \int_{-\infty}^{\infty} e^{-(\alpha X + X^2/2)} dX = \frac{V^2 e^{\alpha^2/2}}{2\nu_0}, \quad (53)$$

where we notice the opposite sign in the exponential argument in comparison to the  $T \rightarrow 0$  limit.

The two limits for  $T$  and the small- $\alpha$  expansion (48) can be interpolated in a compact expression

$$D = \frac{V^2}{2\nu_0} \exp\left[\frac{\alpha^2(\nu_0 T - 1)}{2(\nu_0 T + 1)}\right]. \quad (54)$$

By changing  $T$  between its two limits we change  $\tau \equiv (\nu_0 T - 1)/(\nu_0 T + 1)$  in such a way that  $\tau \in [-1, 1]$  and, hence we have the bounds  $D_{T \rightarrow 0} \leq D \leq D_{T \rightarrow \infty}$ . Simulations with different values of  $\alpha$  and  $T$  show that this interpolating expression is excellent for small  $\alpha$  across distinct orders of  $T$ . Moreover, Eq. (53) turned out to be better than the small- $\alpha$  expansion (48) when used to extrapolate to slightly higher values of  $\alpha$ .

## V. CONCLUSIONS

Here we reviewed and extended general theoretical methods as well as performed simulations to investigate the approach to diffusion of run-and-tumble bacteria

within four models: conventional run-and-tumble, partial reorientation, run-and-reverse with rotational diffusion, and stochastic tumbling rate. By focusing on the mean-squared displacement and on the excess kurtosis both analytically and computationally, we have extracted the effects of basic model parameters on how slowly diffusion is reached. The methods have been presented in a way that makes them easy to be translated into other models of particle dispersal. Although we have worked in 2D for the sake of simplicity, 3D generalizations should be straightforward to perform [5]. Furthermore, since many tracking experiments are performed in quasi-2D geometries [30], our results are directly applicable.

For the conventional RT model we obtained that the excess kurtosis approaches zero exponentially with a rate equal to the tumbling rate  $\nu_0$ . However, for the other models, new time scales appear, which can make the approach to the diffusive regime much slower. For the case of partial reorientation, the new time scales depend on the averages  $\sigma_1 = \langle \cos \theta_s \rangle$  and  $\sigma_2 = \langle \cos 2\theta_s \rangle$  of the tumbling angle  $\theta_s$ , and diverge when either of them approaches one. This happens when the  $\theta_s$  distribution is sharply peaked around both 0 and 180°. For the run-and-reverse model the new time scale is given by the inverse of the rotational diffusivity,  $D_r$ . When  $D_r \ll \nu_0$ , swimmers remain performing a one-dimensional random walk for a long time and transit slowly to the full diffusive motion. Finally, the stochastic tumbling rate model, which describes the dynamics of *E. coli*, is characterized by two parameters: the sensitivity  $\alpha$  of the tumbling rate to the concentration fluctuations of a relevant protein and the memory time  $T$  of this concentration fluctuations. Analytical results are obtained as an expansion for small  $\alpha$ , in which case long relaxation times, eventually diverging, are obtained for long memory times. Simulations are in excellent agreement. In this model we also compute the long-time diffusion coefficient, finding an expression valid for small  $\alpha$  and any value of  $T$ .

Concomitantly, when the relaxation times grow, the

same can happen with the amplitude of the excess kurtosis, implying that the swimmer dispersion remains largely non-Gaussian for long times. The emergence of large relaxation times to reach the vanishing of the excess kurtosis implies that diffusion or reaction–diffusion equations cannot be used to describe bacterial dispersion at intermediate times and distances. Instead, discrete element method simulations could be used. This becomes relevant in the design of microrobots for bioengineering applications [35] which include, for example, killing pathogenic bacteria [36] or removing toxic heavy metals from contaminated water [37].

By simulating with the experimentally obtained *E. coli* values  $\nu_0 = 1.0 \text{ s}^{-1}$  and  $\langle \cos \theta_s \rangle \approx 0.33$  [6], we estimate that the time to reach an excess kurtosis  $\gamma(t)$  such that  $|\gamma(t)| = 0.05$  is  $t \approx 71.2 \text{ s}$ , a value that is independent of the swim speed  $V$ , as expected. A similar analysis can be done for the model with stochastic tumbling rate by using the previously mentioned values  $T = 19.0 \text{ s}$ ,  $\nu_0 = 0.65 \text{ s}^{-1}$ , and  $\alpha = 1.62$ , and by setting  $D_r = 0$  and  $\sigma_1 = 0$  since their values are small [33]. This gives  $|\gamma(t)| = 0.05$  at  $t \approx 143.7 \text{ s}$ .

In future work we will use the methods employed here to compare how several types of interacting [20, 38] swimmers approach diffusion. In particular, because of the richness imparted by polydispersity [39–42], fluid mixtures of interacting run-and-tumble particles with different swimming strategies will be studied. One might also want to tackle circularly propelled active particles and investigate similar associated phenomena including those dependent on the so-called reverse rotations of driven rigid bodies [43, 44].

## VI. ACKNOWLEDGMENTS

This research is supported by Fondecyt Grant No. 1180791 (R.S.) and by the Millennium Nucleus Physics of Active Mater of ANID (Chile).

- 
- [1] Brendan B Larsen, Elizabeth C Miller, Matthew K Rhodes, and John J Wiens. Inordinate fondness multiplied and redistributed: the number of species on earth and the new pie of life. *The Quarterly Review of Biology*, 92(3):229–265, 2017.
  - [2] William B Whitman, David C Coleman, and William J Wiebe. Prokaryotes: the unseen majority. *Proceedings of the National Academy of Sciences*, 95(12):6578–6583, 1998.
  - [3] Stilianos Louca, Florent Mazel, Michael Doebeli, and Laura Wegener Parfrey. A census-based estimate of earth’s bacterial and archaeal diversity. *PLoS Biol*, 17(2):e3000106, 2019.
  - [4] Graham F Hatfull. Dark matter of the biosphere: the amazing world of bacteriophage diversity. *Journal of Virology*, 89(16):8107–8110, 2015.
  - [5] Johannes Taktikos, Holger Stark, and Vasily Zaboruaev. How the motility pattern of bacteria affects their dispersal and chemotaxis. *PLoS ONE*, 8(12):e81936, 2013.
  - [6] Howard C Berg. *Random walks in biology*. Princeton University Press, 1993.
  - [7] Jens Efsen Johansen, Jarone Pinhassi, Nicholas Blackburn, Ulla Li Zweifel, and Åke Hagström. Variability in motility characteristics among marine bacteria. *Aquatic Microbial Ecology*, 28(3):229–237, 2002.
  - [8] Greg M Barbara and James G Mitchell. Bacterial tracking of motile algae. *FEMS Microbiology Ecology*, 44(1):79–87, 2003.
  - [9] Howard C Berg and Douglas A Brown. Chemotaxis in *escherichia coli* analysed by three-dimensional tracking. *Nature*, 239(5374):500–504, 1972.
  - [10] Howard C Berg. *E. coli in Motion*. Springer Science & Business Media, 2008.

- [11] Stephen A Gourley and Yang Kuang. A delay reaction–diffusion model of the spread of bacteriophage infection. *SIAM Journal on Applied Mathematics*, 65(2):550?–566, 2004.
- [12] Nick F Britton. *Reaction–Diffusion Equations and Their Applications to Biology*. Academic Press, 1986.
- [13] Messoud Efeendiev. *Evolution Equations Arising in the Modelling of Life Sciences*. Springer Basel, 2013.
- [14] Yuhai Tu and G Grinstein. How white noise generates power-law switching in bacterial flagellar motors. *Physical Review Letters*, 94(20):208101, 2005.
- [15] Subrata Dev and Sakuntala Chatterjee. Run-and-tumble motion with steplike responses to a stochastic input. *Physical Review E*, 99(1):012402, 2019.
- [16] M Reza Shaebani and Heiko Rieger. Transient anomalous diffusion in run-and-tumble dynamics. *Frontiers in Physics*, 7:120, 2019.
- [17] Andrea Villa-Torrealba, Oscar Paredes-Altuve, and Jhoan Toro-Mendoza. Non-quadratic short-time regime of active brownian deformable droplets. *Submitted*.
- [18] Borge ten Hagen, Sven van Teeffelen, and Hartmut Löwen. Brownian motion of a self-propelled particle. *Journal of Physics: Condensed Matter*, 23(19):194119, 2011.
- [19] Xu Zheng, Borge ten Hagen, Andreas Kaiser, Meiling Wu, Haihang Cui, Zhanhua Silber-Li, and Hartmut Löwen. Non-gaussian statistics for the motion of self-propelled janus particles: Experiment versus theory. *Physical Review E*, 88(3):032304, 2013.
- [20] Stefanie Put, Jonas Berx, and Carlo Vanderzande. Non-gaussian anomalous dynamics in systems of interacting run-and-tumble particles. *Journal of Statistical Mechanics: Theory and Experiment*, 2019(12):123205, 2019.
- [21] K Martens, L Angelani, R Di Leonardo, and L Bocquet. Probability distributions for the run-and-tumble bacterial dynamics: An analogy to the lorentz model. *The European Physical Journal E*, 35(9):84, 2012.
- [22] David Saintillan. The dilute rheology of swimming suspensions: A simple kinetic model. *Experimental Mechanics*, 50(9):1275–1281, 2010.
- [23] David Saintillan. Rheology of active fluids. *Annu. Rev. Fluid Mech.*, 50:563–592, 2018.
- [24] Rodrigo Soto. *Kinetic Theory and Transport Phenomena*. Oxford Master Series in Physics. Oxford University Press, 2016.
- [25] Jean Pierre Boon and Sidney Yip. *Molecular hydrodynamics*. Courier Corporation, 1991.
- [26] Robert Mazo. *Brownian Motion, Fluctuations, Dynamics and Applications*. Oxford Univ. Press, 2002.
- [27] Jonathan Saragosti, Pascal Silberzan, and Axel Buguin. Modeling e. coli tumbles by rotational diffusion. implications for chemotaxis. *PLoS ONE*, 7(4), 2012.
- [28] Pawel Romanczuk, Markus Bär, Werner Ebeling, Benjamin Lindner, and Lutz Schimansky-Geier. Active brownian particles. *The European Physical Journal Special Topics*, 202(1):1–162, 2012.
- [29] Johannes Taktikos, Vasily Zaburdaev, and Holger Stark. Modeling a self-propelled autochemotactic walker. *Physical Review E*, 84(4):041924, 2011.
- [30] Clemens Bechinger, Roberto Di Leonardo, Hartmut Löwen, Charles Reichhardt, Giorgio Volpe, and Giovanni Volpe. Active particles in complex and crowded environments. *Reviews of Modern Physics*, 88(4):045006, 2016.
- [31] Xiaobing Chen and Howard C Berg. Torque-speed relationship of the flagellar rotary motor of escherichia coli. *Biophysical journal*, 78(2):1036–1041, 2000.
- [32] Philippe Cluzel, Michael Surette, and Stanislas Leibler. An ultrasensitive bacterial motor revealed by monitoring signaling proteins in single cells. *Science*, 287(5458):1652–1655, 2000.
- [33] Nuris Figueroa-Morales, Thierry Darnige, Carine Douarche, Vincent Martinez, Rodrigo Soto, Anke Lindner, and Eric Clément. 3d spatial exploration by e. coli echoes motor temporal variability. *arXiv preprint arXiv:1803.01295*, 2018.
- [34] George B Arfken and Hans J Weber. *Mathematical methods for physicists*, 1999.
- [35] Hakan Ceylan, Joshua Giltinan, Kristen Kozielski, and Metin Sitti. Mobile microrobots for bioengineering applications. *Lab on a Chip*, 17(10):1705–1724, 2017.
- [36] Diana Vilela, Morgan M Stanton, Jemish Parmar, and Samuel Sanchez. Microbots decorated with silver nanoparticles kill bacteria in aqueous media. *ACS Applied Materials & Interfaces*, 9(27):22093–22100, 2017.
- [37] Diana Vilela, Jemish Parmar, Yongfei Zeng, Yanli Zhao, and Samuel Sanchez. Graphene-based microbots for toxic heavy metal removal and recovery from water. *Nano letters*, 16(4):2860–2866, 2016.
- [38] Rodrigo Soto and Ramin Golestanian. Run-and-tumble dynamics in a crowded environment: Persistent exclusion process for swimmers. *Physical Review E*, 89(1):012706, 2014.
- [39] Pablo de Castro and Peter Sollich. Phase separation dynamics of polydisperse colloids: a mean-field lattice-gas theory. *Phys. Chem. Chem. Phys.*, 19:22509–22527, 2017.
- [40] Pablo de Castro and Peter Sollich. Critical phase behavior in multi-component fluid mixtures: Complete scaling analysis. *The Journal of Chemical Physics*, 149(20):204902, 2018.
- [41] Pablo de Castro and Peter Sollich. Phase separation of mixtures after a second quench: composition heterogeneities. *Soft Matter*, 15(45):9287–9299, 2019.
- [42] Pablo Souza de Castro Melo. *Phase separation of polydisperse fluids*. 2019.
- [43] Fernando Parisio. Reverse rotations in the circularly driven motion of a rigid body. *Physical Review E*, 78(5):055601, 2008.
- [44] Pablo de Castro and Fernando Parisio. Role of viscous friction in the reverse rotation of a disk. *Physical Review E*, 90(1):013201, 2014.